BIN1 modulation in vivo rescues dynamin-related myopathy

Valentina Maria Lionello, Christine Kretz, Evelina Edelweiss, Corinne Crucifix, Raquel Gómez-Oca, Nadia Messaddeq, Suzie Buono, Pascale Koebel, Xènia Massana Muñoz, Nadège Diedhiou, et al.

BIN1 modulation in vivo rescues dynamin-related myopathy

Valentina Maria Lionello[a], Christine Kretz[a], Evelina Edelweiss[a], Corinne Crucifix[a], Raquel Gómez-Oca[a,b], Nadia Messaddeq[a], Suzie Buono[a], Pascale Koebel[a], Xènia Massana Muñoz[a], Nadège Diedhiou[a], Belinda S. Cowling[a,b], Marc Bitoun[c], and Jocelyn Laporte[a,1]

[a]Institut de Génétique et de Biologie Moléculaire et Cellulaire, INSERM U1258, CNRS UMR 7104, Université de Strasbourg, Illkirch, F-67404, France; [b]Dynacure, Illkirch, F-67400, France; and [c]Institute of Myology, Centre of Research in Myology, INSERM, UMRS 974, Sorbonne Université, F-75013, Paris, France

Edited by Se-Jin Lee, Genetics and Genome Sciences, University of Connecticut School of Medicine, Farmington, CT; received May 25, 2021; accepted January 18, 2022

The mechanoenzyme dynamin 2 (DNM2) is crucial for intracellular organization and trafficking. *DNM2* is mutated in dominant centronuclear myopathy (DNM2-CNM), a muscle disease characterized by defects in organelle positioning in myofibers. It remains unclear how the in vivo functions of DNM2 are regulated in muscle. Moreover, there is no therapy for DNM2-CNM to date. Here, we overexpressed human amphiphysin 2 (BIN1), a membrane remodeling protein mutated in other CNM forms, in *Dnm2*$^{RW/+}$ and *Dnm2*$^{RW/RW}$ mice modeling mild and severe DNM2-CNM, through transgenesis or with adeno-associated virus (AAV). Increasing BIN1 improved muscle atrophy and main histopathological features of *Dnm2*$^{RW/+}$ mice and rescued the perinatal lethality and survival of *Dnm2*$^{RW/RW}$ mice. In vitro experiments showed that BIN1 binds and recruits DNM2 to membrane tubules, and that the BIN1-DNM2 complex regulates tubules fission. Overall, BIN1 is a potential therapeutic target for dominant centronuclear myopathy linked to DNM2 mutations.

congenital myopathy | membrane remodeling | gene therapy | dynamin | amphiphysin

Membrane remodeling is a key process for intracellular organization and intercellular communication. A number of proteins regulating this process are mutated in human diseases. We focus on centronuclear myopathy due to mutations in the large GTPase dynamin 2 (DNM2), the first protein shown to catalyze membrane fission (1, 2). The pathological implication of DNM2 is unclear and there is no therapy to date for this disease. Here we validated an approach that ameliorated the disease in a mouse model and investigated the pathological and rescue mechanisms.

DNM2 is a mechanoenzyme implicated mainly in vesicle budding in endocytosis and recycling and in cytoskeleton organization (1, 3). Upon membrane binding DNM2 oligomerizes around the neck of nascent vesicles, and the increase in the GTPase activity correlates with membrane fission. Several SH3 (Src homology 3) containing proteins as endophilins or amphiphysins can bind to the proline-rich domain (PRD) of dynamins. Among these, BIN1 is a N-BAR (N-terminal amphipathic helix Bin Amphiphysin Rvs) domain protein sensing and promoting membrane curvature and tubulation (4, 5). BAR-SH3 proteins recruit dynamins to membranes and promote their functions at specific sites (6). Recent findings suggested endophilin structurally inhibits dynamin-mediated membrane fission (7). However, it remains unclear how BAR proteins modulate dynamins activity and functions, especially in vivo.

Centronuclear myopathies (CNMs) are rare congenital myopathies linked to muscle weakness, hypotonia, and muscle atrophy correlated with hypotrophic muscle fibers and mislocalized or altered organelles as nuclei, mitochondria, and triads (8, 9). Apart from DNM2, loss-of-function mutations in the membrane remodeling protein amphiphysin 2 (BIN1; MIM [Mendelian Inheritance in Man]# 255200) (10), in the lipid phosphatase myotubularin (MTM1; MIM#310400) (11) and in the triad calcium channel ryanodine receptor (RYR1; MIM#117000) (12–14), lead to CNMs. The incidence of CNM is about 24 per million births, leading to a calculated prevalence for DNM2-CNM of about 550 in total for the European Union, the United States, Australia, and Japan (15). Heterozygous *DNM2* mutations cause dominant CNMs (MIM#160150), ranging from severe muscle involvement with neonatal onset to mild phenotype with adult onset, partly correlating with the site of mutation (16). A homozygous DNM2 mutation was reported in patients with recessive lethal congenital contracture syndrome (LCCS5; MIM#615368) while their heterozygous parents displayed a mild CNM (17). Several lines of evidence suggest that DNM2-CNM mutations are gain of function. They increase the GTPase activity and oligomer stability in vitro (18, 19). Moreover, in vivo, overexpression of wild-type (WT) DNM2 cause a CNM-like phenotype in mice (20, 21). Human and mouse genetics suggested that the BIN1-DNM2 complex is important for skeletal muscle. In particular, some BIN1-CNM mutations abrogate the binding to DNM2 while others decrease the membrane tubulation properties of BIN1 (10). Moreover, the perinatal lethality of *Bin1*$^{-/-}$ mice was rescued by decreasing *Dnm2* levels to 50% (22).

BIN1 overexpression was shown to rescue MTM1-CNM in mice (23). Here, we hypothesize that modulating BIN1 can rescue the muscular phenotypes due to DNM2-CNM mutations. As a DNM2-CNM model, we selected the *Dnm2*$^{RW/+}$ mouse

Significance

Membrane remodeling and trafficking is essential for intracellular organization under normal conditions and can be altered in a plethora of diseases. Here we characterized the action of amphiphysin (BIN1) and dynamin (DNM2), two main regulators of membrane remodeling mutated in congenital myopathies. We found their interplay is necessary for membrane fission in vitro and to maintain muscle homeostasis in vivo. Moreover, increasing BIN1 expression was validated as a therapeutic approach to ameliorate both mild and severe forms of DNM2-associated myopathies in mice.

Author contributions: J.L. conceived and supervised the project; V.M.L., E.E., C.C., B.S.C., and J.L. designed research; V.M.L., C.K., E.E., C.C., R.G.-O., N.M., S.B., P.K., X.M.M., N.D., and B.S.C. performed research; M.B. contributed new reagents/analytic tools; V.M.L., E.E., B.S.C. and J.L. analyzed data; and V.M.L. and J.L. wrote the paper.

Competing interest statement: B.S.C. and J.L. are co-founders of Dynacure. R.G.-O., S.B., and B.S.C. are currently employed by Dynacure.

This article is a PNAS Direct Submission.

[1]To whom correspondence may be addressed. Email: jocelyn@igbmc.fr.

This article contains supporting information online at http://www.pnas.org/lookup/suppl/doi:10.1073/pnas.2109576119/-/DCSupplemental.

Published February 25, 2022.

that mimics the most common CNM mutation, R465W, in the middle/stalk domain, and displays a mild muscle weakness with decreased muscle force, muscle atrophy due to myofiber hypotrophy, and central accumulation of oxidative staining from 2 mo of age (24). *Dnm2*$^{RW/+}$ mice do not display centralized nuclei in myofibers unlike patients; albeit myonuclei domains seem altered (25). The homozygous *Dnm2*$^{RW/RW}$ mice developed a more severe phenotype and died at birth potentially from hypoglycemia and altered neonatal autophagy (25).

In this study, we overexpressed human BIN1 in *Dnm2*$^{RW/+}$ and *Dnm2*$^{RW/RW}$ mice, which model mild and severe forms of DNM2-CNM, respectively. Of note, we validate the proof of concept that increasing BIN1 rescues DNM2-CNM and decipher the regulation of the BIN1-DNM2 complex in vitro and in vivo.

Results

BIN1 Overexpression Improves *Dnm2*$^{RW/+}$ Force and Muscle Atrophy. To study the effect of BIN1 overexpression on a DNM2-CNM mutation in vivo, female *Dnm2*$^{RW/+}$ mice were crossed with transgenic (Tg)*BIN1* mice expressing human *BIN1* from a bacterial artificial chromosome (BAC) to produce *Dnm2*$^{RW/+}$ Tg*BIN1* mice. BIN1 protein level was measured and a twofold increase of total BIN1 proteins was detected in *Dnm2*$^{RW/+}$ Tg*BIN1* compared to *Dnm2*$^{RW/+}$ (*SI Appendix*, Fig. S1*A*).

Most analyzed mice survived until killing at the age of 4 or 8 mo old and no body weight difference was identified between the different genotypes studied: WT, Tg*BIN1*, *Dnm2*$^{RW/+}$, and *Dnm2*$^{RW/+}$ Tg*BIN1* (Fig. 1*A*). Hanging and rotarod tests were performed at different time points. *Dnm2*$^{RW/+}$ mice exhibited a significant defect in hanging time, while *Dnm2*$^{RW/+}$ Tg*BIN1* mice performed similarly to WT and Tg*BIN1* controls (Fig. 1*B* and *SI Appendix*, Fig. S2*A*). No difference was observed in the rotarod test between all genotypes at 4 and 8 mo (*SI Appendix*, Fig. S2 *B* and *C*). The overexpression of BIN1 significantly rescued the tibialis anterior (TA) muscle atrophy of *Dnm2*$^{RW/+}$ mice (Fig. 1*C*). The TA is the most affected skeletal muscle in CNM animal models and therefore is the most studied. No difference was measured between *Dnm2*$^{RW/+}$ and WT in soleus and gastrocnemius muscles (*SI Appendix*, Fig S2 *D* and *E*). To conclude, *Dnm2*$^{RW/+}$ Tg*BIN1* mice exhibited a slight improvement in body strength and a complete rescue of the muscle atrophy compared to the *Dnm2*$^{RW/+}$ disease model.

BIN1 Improves *Dnm2*$^{RW/+}$ CNM Histological Features. We next investigated the histological and ultrastructural features of *Dnm2*$^{RW/+}$ and *Dnm2*$^{RW/+}$ Tg*BIN1* to correlate with the muscle atrophy. Transversal TA sections were stained with hematoxylin and eosin (H&E). At 4 mo, *Dnm2*$^{RW/+}$ Tg*BIN1* muscles showed a tendency for more large fibers than *Dnm2*$^{RW/+}$ muscles (Fig. 1*D* and *SI Appendix*, Fig. S2 *F–H*). As previously reported, the main histological phenotype of *Dnm2*$^{RW/+}$ mice was the central accumulation of oxidative activity (Fig. 1*E*) (24). This finding was confirmed upon succinate dehydrogenase (SDH) and nicotinamide adenine dinucleotide tetrazolium reductase (NADH-TR) staining and quantification of the central accumulations (Fig. 1*E* and *SI Appendix*, Fig. S2*I*, arrowheads). The overexpression of BIN1 in *Dnm2* $^{RW/+}$ mice restored the WT phenotype (Fig. 1*F*).

Skeletal muscle ultrastructure was investigated by electron microscopy. *Dnm2*$^{RW/+}$ muscle presented enlarged mitochondria that were often found clustered, correlating with the accumulation of oxidative staining (*SI Appendix*, Fig. S3 *A* and *B*). Mitochondria organization was ameliorated upon BIN1 overexpression (Fig. 1*G*). Transverse tubule (T-tubule) transversal section was rounder in *Dnm2*$^{RW/+}$ and *Dnm2*$^{RW/+}$ Tg*BIN1* mice compared to WT (Fig. 1 *H* and *I*). We excluded that this phenotype is due to the overexpression of BIN1 as previous analysis did not identify triad abnormalities in the Tg*BIN1* (23). However, T-tubule orientation was altered and more longitudinal in *Dnm2*$^{RW/+}$ mice and rescued in *Dnm2*$^{RW/+}$ Tg*BIN1* mice (Fig. 1*J*). Furthermore, *Dnm2*$^{RW/+}$ muscle displayed abnormal dihydropyridine receptor (DHPR) staining. DHPR is a Ca^{2+} channel localized on the T-tubule in skeletal muscle and plays a fundamental role in excitation–contraction coupling necessary for skeletal muscle contraction. DHPR localization was rescued in *Dnm2*$^{RW/+}$ Tg*BIN1* (Fig. 1*K* and *SI Appendix*, Fig. S3*C*). Overall, the overexpression of BIN1 rescued the abnormal mitochondria and T-tubule organization representing the main histopathological features in common between the *Dnm2*$^{RW/+}$ mice and DNM2-CNM human patients.

Postnatal Overexpression of BIN1 Improves *Dnm2*$^{RW/+}$ Muscle Atrophy and Histological Features. *Dnm2*$^{RW/+}$ Tg*BIN1* mice were obtained by genetic cross, resulting in BIN1 overexpression starting in utero. To develop a translated therapeutic approach and modulate BIN1 expression after birth, we overexpressed the human BIN1 isoform corresponding to the main isoform detected in adult skeletal muscle in mice and human (26). BIN1 was overexpressed using adeno-associated virus (AAV) injected intramuscularly in 3-wk-old *Dnm2*$^{RW/+}$ mice that were subsequently analyzed 4 wk postinjection. A fourfold increase in BIN1 expression was detected in muscles from *Dnm2*$^{RW/+}$ mice injected with AAV-*BIN1* compared to the contralateral leg injected with control AAV (AAV-Ctrl) (Fig. 2*A*). Exogenous BIN1 expression correlated with a tendency to increase the TA muscle weight in *Dnm2*$^{RW/+}$ leg compared to the contralateral injected with AAV-Ctrl in 7-wk-old mice (Fig. 2*B*).

Since a main phenotype of the *Dnm2*$^{RW/+}$ mice is histopathological alteration, we investigated the effect of acute BIN1 overexpression on the muscle organization. At 7 wk old (4 wk of treatment), increase in fiber size was noted in the *Dnm2*$^{RW/+}$ injected with AAV-*BIN1* compared to *Dnm2*$^{RW/+}$ TA injected with AAV-Ctrl (Fig. 2 *C–F*). In addition, the injection of AAV-*BIN1* ameliorated the central accumulation of NADH-TR and SDH staining observed in *Dnm2*$^{RW/+}$ TA muscles injected with AAV-Ctrl (Fig. 2 *G–I*). In summary, the acute expression of human BIN1 in *Dnm2*$^{RW/+}$ TA muscle improved different histopathology hallmarks after only 4 wk of expression.

Overexpression of BIN1 Prevents the Premature Lethality of *Dnm2*$^{RW/RW}$ Mice. As the overexpression of BIN1 was sufficient to improve the *Dnm2*$^{RW/+}$ muscle atrophy and histopathology, we next tested whether the overexpression of BIN1 rescues the more severe phenotype of *Dnm2*$^{RW/RW}$ homozygous mice, which die at birth (24). To address this question *Dnm2*$^{RW/RW}$ mice overexpressing human BIN1 were generated (*Dnm2*$^{RW/RW}$ Tg*BIN1*). At postnatal day 10 (P10), only 0.7% of the pups analyzed were *Dnm2*$^{RW/RW}$ mice, suggesting that the majority died prior to P10, while 18.1% were *Dnm2*$^{RW/RW}$ Tg*BIN1*, corresponding to the expected Mendelian ratio (*SI Appendix*, Table S1). All *Dnm2*$^{RW/RW}$ Tg*BIN1* mice survived until the end of the full study at 2 mo (Movie S1). A small cohort of *Dnm2*$^{RW/RW}$ Tg*BIN1* mice were followed up and strikingly survived until 18 mo, which was the last timepoint analyzed (Movie S2). Western blot showed a 2.6-fold BIN1 overexpression in *Dnm2*$^{RW/RW}$ Tg*BIN1* mice (*SI Appendix*, Fig. S4*A*). Overall, increasing BIN1 expression was sufficient to rescue the neonatal lethality and lifespan of *Dnm2*$^{RW/RW}$ mice.

Characterization of *Dnm2*$^{RW/RW}$ Mice Overexpressing Human BIN1. As the overexpression of BIN1 rescued the *Dnm2*$^{RW/RW}$ survival, we characterized their growth, motor function, and muscle phenotypes at 2 mo. No difference was observed

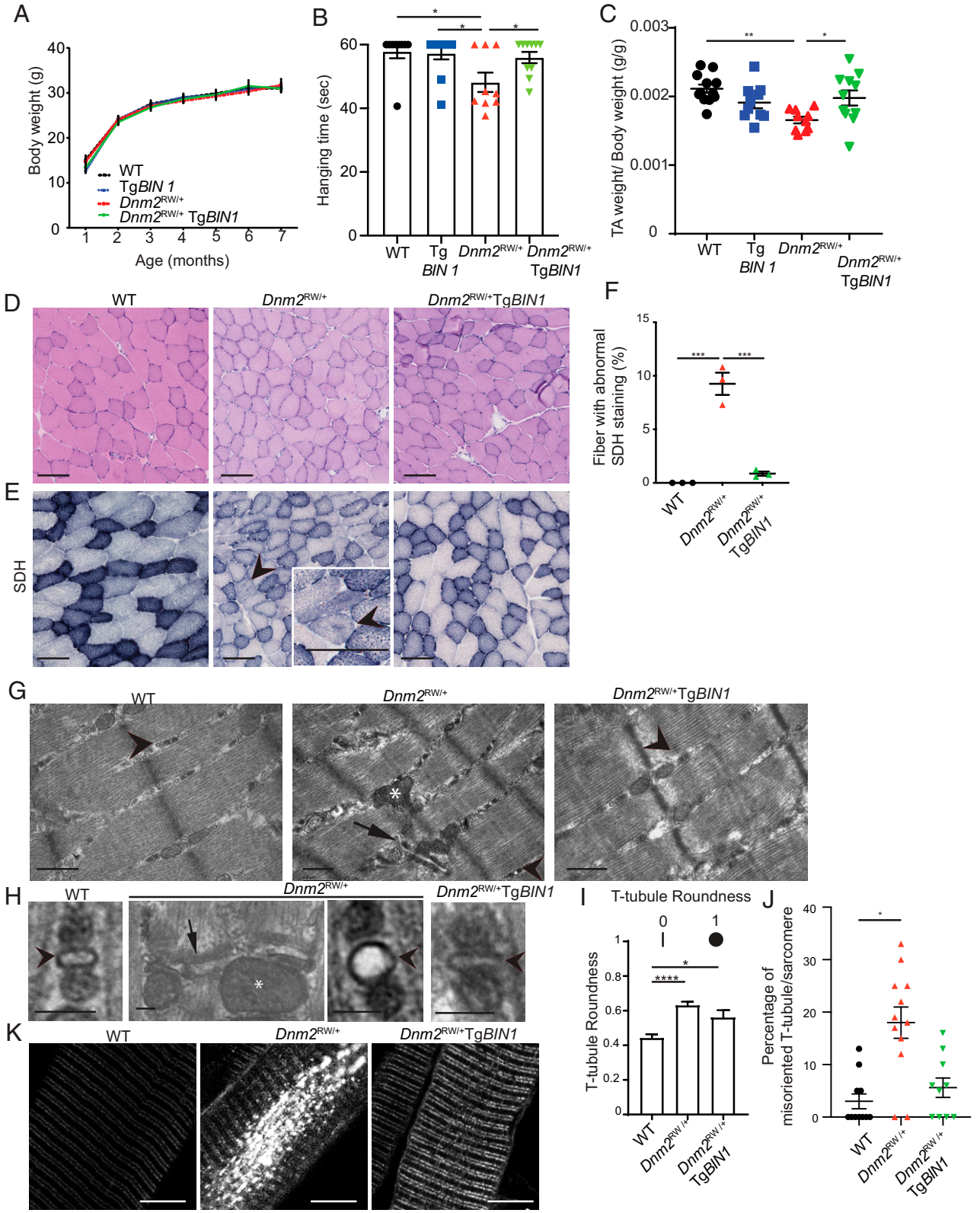

Fig. 1. Overexpressing BIN1 ameliorates the histopathology of *Dnm2*$^{RW/+}$ mice. (*A*) Body weight with age ($n > 5$). (*B*) Hanging test at 3 mo: mice were suspended from a cage lid for a maximum of 60 s and each mouse repeated the test three times ($n > 5$). (*C*) Weight of TA muscle normalized on total body weight. (*D*) Transversal TA muscle sections stained with H&E. (*E*) Transversal TA muscle sections stained with SDH. SDH staining specifically labels mitochondria oxidative activity. (Scale bar, 100 μm.) (*F*) Percentage of fibers with abnormal SDH staining at 4 mo. (*G*) Longitudinal TA muscle ultrastructure observed by electron microscopy. Triads (arrowheads), longitudinal oriented T-tubule (arrow), enlarged mitochondria (star). (Scale bar, 0.5 μm.) (*H*) High-magnification view of the triads. (Scale bar, 0.1 μm.) (*I*) Quantification of T-tubules roundness ($n \geq 2$, $n \geq 29$). (*J*) Quantification of misoriented T-tubules ($n = 3$; n sarcomere >30). (*K*) Longitudinal TA muscle section stained with DHPR antibody; note the abnormal DHPR distribution in *Dnm2*$^{RW/+}$ muscle. Statistical test: one-way ANOVA; Tukey's post hoc test. $^{*}P < 0.05$, $^{**}P < 0.01$, $^{***}P < 0.001$, $^{****}P < 0.0001$.

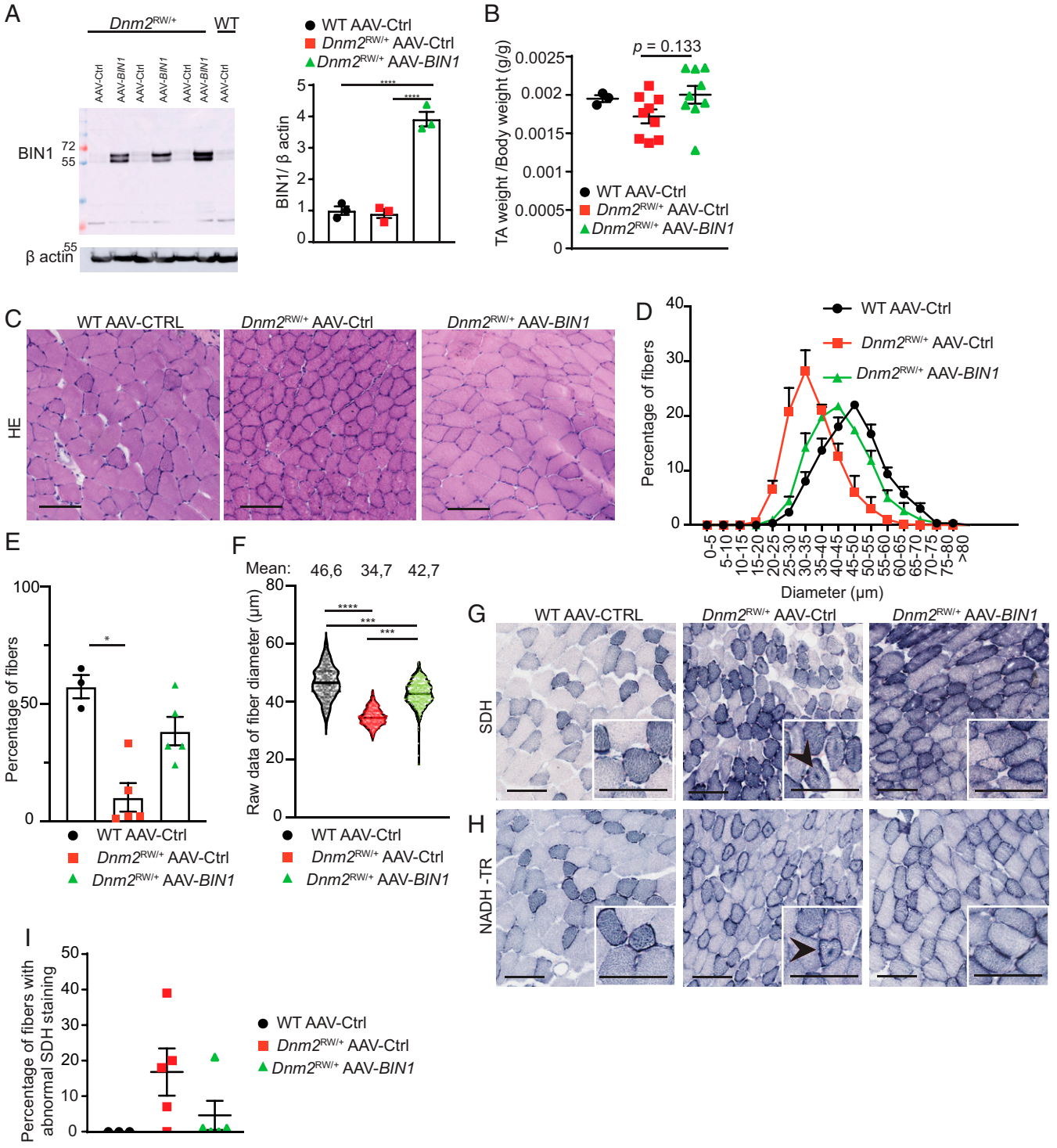

Fig. 2. Postnatal intramuscular overexpression of BIN1 improves the histopathology of *Dnm2* $^{RW/+}$ mice. *Dnm2*$^{RW/+}$ mice were injected at 3 wk old with either AAV empty (AAV-Ctrl) in one TA muscle or AAV-*BIN1* in the contralateral TA, and mice were analyzed 4 wk postinjection. (*A*) Western blot with anti-BIN1 antibody. BIN1 level was normalized on beta-actin. (*B*) TA muscle weight normalized on total body weight ($n \geq 3$). (*C*) Transversal TA sections stained with H&E. (Scale bar, 100 µm.) (*D*) Minimum Feret diameter of TA fibers grouped into 5-µm intervals ($n \geq 3$) and (*E*) percentage of fibers with a minimum Feret diameter >45 µm. (*F*) Mean Feret diameter presented as a violin plot. Transversal TA sections stained with (*G*) SDH and (*H*) NADH-TR. (*I*) Percentage of fibers with abnormal SDH staining at 4 mo. (Scale bar, 0.5 µm.) Statistical test: Kruskal–Wallis test; Dunn's post hoc. *$P < 0.05$, ***$P < 0.001$, ****$P < 0.0001$.

between WT and *Dnm2*$^{RW/RW}$ Tg*BIN1* regarding the body weight until 6 wk. From 6 wk old, *Dnm2*$^{RW/RW}$ Tg*BIN1* mice weighed less than WT controls (Fig. 3*A*). To assess total body strength, the hanging test was performed at 2 mo and no difference was observed between the *Dnm2*$^{RW/RW}$ Tg*BIN1* and WT mice (Fig. 3*B*). *Dnm2*$^{RW/RW}$ Tg*BIN1* mice had decreased

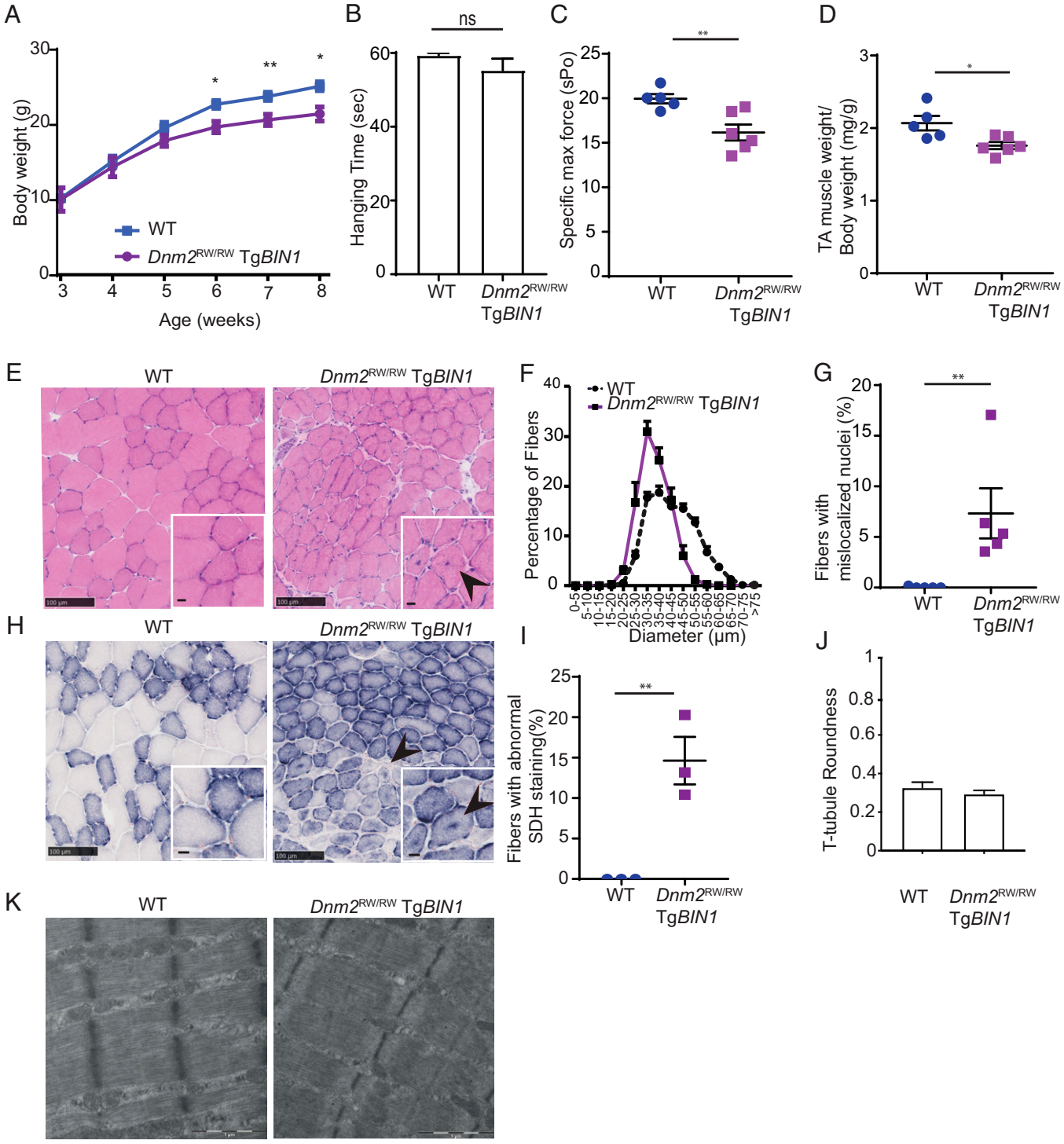

Fig. 3. BIN1 overexpression rescues the survival of *Dnm2* $^{RW/RW}$ mice. (*A*) Body weight with age ($n > 5$). (*B*) Hanging time at 2 mo, topped to 60 s ($n > 5$). (*C*) Specific maximal force of the TA muscles. (*D*) Weight of TA muscle normalized on total body weight ($n > 5$). (*E*) Transversal TA muscle sections stained with H&E. Arrowhead points to a central nucleus. (Scale bar, 100 µm.) (*F*) Minimum Feret diameter of TA fibers grouped into 5-µm intervals ($n = 5$). (*G*) Frequency of muscle fibers with internalized nuclei ($n = 5$). (*H*) Transversal TA muscle sections stained with SDH. Arrowhead points to central accumulation of oxidative activity. (Scale bar, 100 µm.) (*I*) Percentage of fibers with abnormal SDH staining ($n = 3$). (*J*) Quantification of T-tubule roundness ($n = 2$, $n > 12$). (*K*) TA muscle ultrastructure observed by electron microscopy. (Scale bar, 1 µm.) Statistical test: Student's *t* test. ns: not significant, $*P < 0.05$, $**P < 0.01$.

muscle force and smaller TA muscles compared to WT (Fig. 3 *C* and *D*).

To assess the muscle histology, TA muscles were stained with H&E and showed reduced fiber diameter in *Dnm2*$^{RW/RW}$ Tg*BIN1* mice compared to WT (Fig. 3 *E* and *F*). In addition, a small percentage of fibers with internalized or centralized nuclei (around 7%) were noted in *Dnm2*$^{RW/RW}$ Tg*BIN1* TA muscles (Fig. 3*G*), while this CNM phenotype was not observed in *Dnm2*$^{RW/+}$ mice (Fig. 2) (24). Moreover, abnormal central accumulation of oxidative activity (SDH staining) was visible in

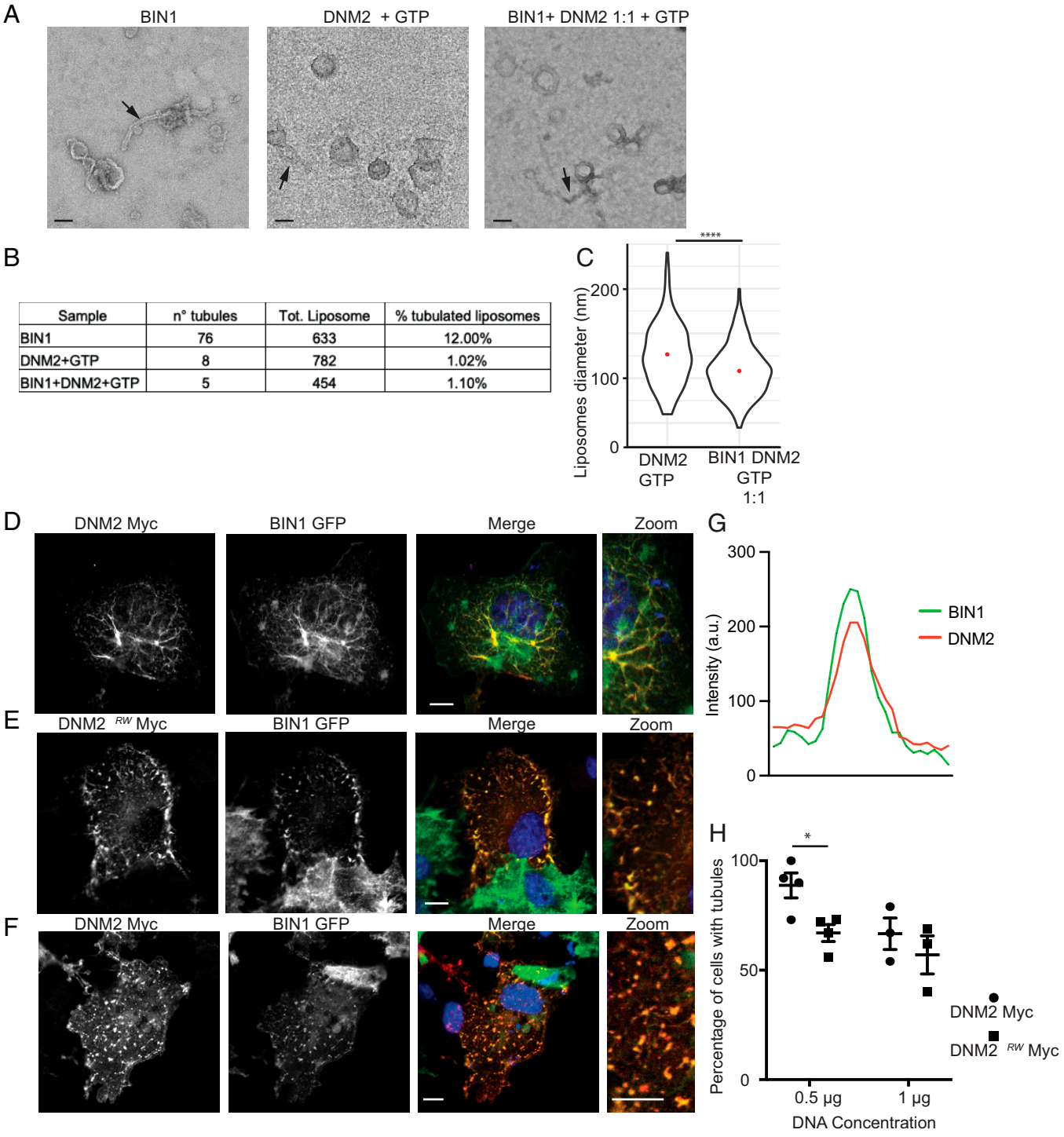

Sample	n° tubules	Tot. Liposome	% tubulated liposomes
BIN1	76	633	12.00%
DNM2+GTP	8	782	1.02%
BIN1+DNM2+GTP	5	454	1.10%

Fig. 4. Activity of BIN1 and DNM2 on membrane tubulation and fission. (*A*) Negative staining and electron microscopy of liposomes incubated with purified BIN1, DNM2 + GTP, or BIN1 + DNM2 + GTP (1:1 ratio of BIN1:DNM2). Arrows point to membrane tubules. (Scale bar, 200 nm.) (*B*) Quantification of the number of membrane tubules emanating from liposomes. (*C*) Quantification of liposome diameter after incubation with DNM2 + GTP or BIN1 + DNM2 + GTP (1:1 ratio of BIN1:DNM2); liposomes analyzed, $n > 150$. (*D*) COS-1 cells transfected with BIN1 (green) and DNM2 WT (red) or (*E*) BIN1 and $DNM2^{RW}$ with 0.5 µg DNM2 construct DNA, or (*F*) transfected with BIN1 and DNM2 WT with 1 µg DNM2 construct DNA. (*G*) BIN1 and DNM2 colocalization plot on tubule. (*H*) Percentage of cells with BIN1 tubules after transfection with either 0.5 or 1 µg of DNM2 WT or $DNM2^{RW}$ ($n = 3$). Statistical test: Non-parametric Mann–Whitney test (*C*) and Student's *t* test (*G*). $*P < 0.05$, $****P < 0.0001$.

around 15% of fibers in *Dnm2*$^{RW/RW}$ Tg*BIN1* mice (Fig. 3 *H* and *I*, arrowhead).

Electron microscopy did not reveal strong abnormalities in the sarcomere organization in *Dnm2*$^{RW/RW}$ Tg*BIN1* mice and showed aligned Z-lines and normal muscle T-tubule localization and shape (Fig. 3 *J* and *K*), unlike in the heterozygous *Dnm2*$^{RW/+}$ mice (Fig. 1). In conclusion, *Dnm2*$^{RW/RW}$ Tg*BIN1* mice survived and exhibited the most histological phenotypes

found in the *Dnm2*$^{RW/+}$ mice, reminiscent of the mild form of DNM2-CNM.

BIN1 and DNM2 Form a Complex Regulating Membrane Tubulation. The above data support the idea that BIN1 could be a modulator of DNM2. To better decipher their functional interaction at the molecular level, experiments were conducted in vitro and in cells. The interaction between human DNM2 and human BIN1 was tested by pulldown of recombinant DNM2 produced in insect cells with recombinant GST-BIN1 (glutathione S-transferase BIN1 full length) or GST-SH3 (SH3 domain of BIN1) produced in bacteria (*SI Appendix*, Fig. S5 *A* and *B*). We found BIN1 directly binds DNM2 through the SH3 domain. Increasing the amount of recombinant GST-SH3 correlated with a higher amount of DNM2 WT and DNM2 RW pulled down, supporting the idea that increasing BIN1 sequesters more DNM2 while this interaction is not impacted by the DNM2 R465W CNM mutant. Moreover, the BIN1 SH3 domain was able to pull down the DNM2 R465W CNM mutant from *Dnm2*$^{RW/+}$ muscle extracts, suggesting the direct interaction found in the previous in vitro assays is also present in a muscle context (*SI Appendix*, Fig. S5*C*).

To investigate the function regulated by the BIN1-DNM2 complex, we tested membrane tubulation, a process in which both proteins were previously implicated (27). Liposomes supplemented with phosphatidylserine and PtdIns(4,5)P_2 were incubated with BIN1, DNM2, or BIN1 and DNM2, and analyzed by negative staining. BIN1 generated membrane tubules from liposomes (12% tubulating liposomes) while nearly no tubules were noted with DNM2 + GTP (1% tubulating liposomes) (Fig. 4 *A* and *B*). Addition of DNM2 + GTP to BIN1 in a 1:1 ratio resulted in lack of tubulation (1.1% tubulating liposomes), suggesting DNM2 either prevented or cut the tubules made by BIN1. To distinguish between the two possibilities, the mean diameter of the resulting liposomes was measured and found reduced when DNM2 + GTP was added to BIN1 compared to DNM2 + GTP alone, suggesting DNM2 cut the membrane tubules (Fig. 4*C*; DNM2 alone: 126.6 ± 2.8 nm diameter; DNM2 + BIN1: 108.3 ± 1.9 nm). Overall, these data support the idea that BIN1 and DNM2 work together to regulate membrane tubule fission.

The DNM2 R465W CNM Mutation Alters the Fission Properties of DNM2 in Cells. To confirm that the BIN1-DNM2 complex regulates membrane tubulation in living cells, BIN1 ± DNM2 were overexpressed in cultured cells. BIN1 expression induced intracellular membrane tubules mainly originating from the plasma membrane (*SI Appendix*, Fig. S6*A*), as previously shown (5, 28). At a low DNA concentration, transfected DNM2 WT protein was recruited by and colocalized with BIN1 on tubules (Fig. 4 *D* and *G*), while BIN1 tubules were fragmented upon cell transfection with a higher concentration of DNM2 DNA (Fig. 4*F*). In this last case, BIN1 and DNM2 colocalized to intracellular dots probably representing the product of tubule fission. Altogether, it supported the idea that BIN1 recruits DNM2 to the tubules and that DNM2 can fission membrane as suggested by the liposome data. Coexpression of BIN1 with DNM2 R465W CNM mutant at low DNA concentration led to a lower number of cells with tubules compared to coexpression with DNM2 WT, suggesting this CNM mutant is more potent for membrane fission (Fig. 4 *E*–*H*). The SH3 domain of BIN1 was necessary to recruit DNM2 to the tubules, because a BIN1 ΔSH3 protein lacking the SH3 domain was not able to recruit DNM2 to the membrane tubules (*SI Appendix*, Fig. S6*B*). Increasing concentration of BIN1 (0.25 μg, 0.5 μg, and 1 μg) while maintaining a stable DNM2 R465W concentration (0.5 μg) was linked to a higher percentage of tubulating cells, supporting the idea that BIN1 can prevent the membrane fission by the DNM2 R465W CNM mutant (*SI Appendix*, Fig. S7 *A* and *B*). In conclusion, membrane tubulation in cultured cells is negatively impacted by the DNM2-CNM mutant and improved by BIN1.

Discussion

In this study, we report that exogenous overexpression of human BIN1 ameliorates the muscle phenotype of *Dnm2*$^{RW/+}$ mice, the mammalian model for centronuclear myopathy linked to DNM2 mutations and the perinatal lethality of homozygous *Dnm2*$^{RW/RW}$ mice. These data suggest increasing BIN1 as a therapy for mild and severe forms of centronuclear myopathy linked to DNM2. In addition, in vitro and cell experiments supported that: BIN1 directly binds DNM2, is necessary for its recruitment to membrane tubules, and that the BIN1-DNM2 complex regulates membrane tubule fission.

BIN1 as an In Vivo Modulator of DNM2. The link between BIN1 and DNM2 was barely studied in vivo. The fact that overexpression of BIN1 in the *Dnm2*$^{RW/+}$ mice rescued the muscle phenotypes correlates with the finding that decreasing DNM2 in the *Bin1*$^{-/-}$ mouse rescued its perinatal lethality (22). Thus, modulating the level of either BIN1 or DNM2 compensates for the defects due to the alteration of DNM2 or BIN1, respectively. Based on this study and previous observations in vitro, it is conceivable that BIN1 and DNM2 act together on membrane tubule fission. BIN1 and DNM2 bind together directly through their SH3 and PRD domains, respectively (this study and refs. 4, 5) and recent data suggested that multimerization of SH3 domains together with the presence of multiple SH3 binding sites in the dynamin PRD increases the recruitment of dynamins to membranes (29). Dynamin activity on membranes may then be regulated by BAR-SH3 proteins and the clustering of PIP2 induced by BIN1 (30). In cells, DNM2 is recruited to BIN1-induced membrane tubules, and increasing DNM2 promoted membrane fission (Fig. 4 *D*–*G*). Similarly, the addition of DNM2 to BIN1 on liposomes led to reduction in liposome size and membrane tubule number (Fig. 4 *A*–*C*). These data and hypothesis are in agreement with the study by Chin et al. (31) focused on dynamin, and other studies using other N-BAR proteins as amphiphysin 1 or endophilin together with different dynamins (32, 33).

The R465W DNM2 mutation leads to an increased GTPase activity and membrane fission in vitro (18, 19, 31). Moreover, the DNM2-CNM mutant R465W alters DNM2 fission activity in cells, while increasing BIN1 concentration counteracts this effect (Fig. 4). We verified the BIN1 SH3 domain directly binds the DNM2 R465W CNM mutant in vitro and pulled down DNM2 from *Dnm2*$^{RW/+}$ muscle, suggesting a similar regulation takes place in vivo. Indeed, BIN1 can modulate specifically the effects of this CNM mutant in vivo as, for example, overexpression of BIN1 rescued the lifespan of the homozygous *Dnm2*$^{RW/RW}$ mice and ameliorated the muscle phenotypes of the *Dnm2*$^{RW/+}$ mice (Figs. 1–3). Overall, BIN1 and DNM2 act together on membrane tubule fission and the DNM2-CNM mutation alters this process probably through a gain-of-function mechanism. We hypothesize that, in muscle, BIN1 would induce membrane curvature, recruits DNM2 to these membrane sites, and controls its fission activity that is increased by the DNM2-CNM mutation. We cannot exclude the rescuing effect of BIN1 overexpression in vivo as independent of DNM2.

In cardiac and skeletal muscle, BIN1 was proposed to regulate T-tubule biogenesis. T-tubules are plasma membrane invagination crucial for excitation–contraction coupling and intracellular calcium release. Alteration of T-tubule and triad orientation and shape was noted in the *Dnm2*$^{RW/+}$ mice (Fig. 1), in WT mice transduced with AAV overexpressing the R465W DNM2-CNM mutant (20, 34), and in *Drosophila* and zebrafish overexpressing the same mutant (31, 35). It is thus possible that the BIN1-DNM2 complex regulates

T-tubule biogenesis and/or maintenance. However, we cannot exclude the possibility that this complex also regulates other cellular functions, as expression of BIN1 clearly rescued the central accumulation of mitochondria oxidative activity in myofibers, a hallmark of CNM (Figs. 2 and 3).

Increasing BIN1 as a Therapy to Counteract DNM2 Mutations. We report exogenous expression of BIN1 rescued the DNM2-CNM model through a genetic cross as a proof of concept and then through AAV9 delivery after birth as a translated approach (Figs. 1 and 2). Importantly, several AAV serotypes are already used in clinical trials and the AAV9-based Zolgensma is already commercially available to treat a neuromuscular disease, spinal muscular atrophy (https://www.avexis.com). The human BIN1 gene and cDNA were used here as a first step toward further preclinical development. The Tg*BIN1* mouse we used here was shown to express the muscle-specific isoform 8 in muscle (23); thus we also expressed this isoform through AAV in the present study. The different technical approaches significantly ameliorated the muscle atrophy and the histopathology of the *Dnm2*$^{RW/+}$ mice, major hallmarks of DNM2-CNM in humans (2, 9). BIN1 overexpression also rescued the perinatal death and lifespan of *Dnm2*$^{RW/RW}$ mice (*SI Appendix*, Table S1). Interestingly, the *Dnm2*$^{RW/RW}$ Tg*BIN1* mice had muscle atrophy and central accumulation of nuclei and oxidative activity in myofibers, not affecting their survival. Noteworthy, these alterations are similar to those observed in the untreated *Dnm2*$^{RW/+}$ mice, suggesting BIN1 expression transforms a severe DNM2-CNM disease into a very mild disease form. These data also support the idea that BIN1 expression could ameliorate both the childhood onset DNM2-CNM form mainly due to R465W mutations and the severe neonatal form mainly due to other missense mutations or homozygous mutation (16, 17).

Importantly, BIN1 exogenous expression can ameliorate both DNM2-CNM (this study) and myotubular myopathy, which is considered as the X-linked form of CNM, and is due to mutations in the lipid phosphatase MTM1 (23). Thus, BIN1 represents a common therapeutic target for different myopathy forms, extending the number of patients who may benefit from this potential therapy. It is also an example of a cross-therapy where expression of a CNM gene (as *BIN1*) can ameliorate other myopathies due to mutations in different genes (as *MTM1* and *DNM2*). DNM2 mutations were also reported in autosomal dominant Charcot-Marie-Tooth neuropathy (CMT; MIM#606482) (36), spastic paraplegia (37), and in T-cell lymphoblastic leukemia in combination with *NOTCH1* and *PHD6* mutations (38). The effects of overexpressing BIN1 in models for these diseases remain to be tested. Indeed, it is yet unclear whether DNM2 mutations have a similar functional impact in these diseases as in CNM. Moreover, we validated here the therapeutic potential of the muscle-specific BIN1 isoform for CNM and it remains to be determined whether this specific isoform is functional in the peripheral nervous system and T cells or whether the use of other BIN1 isoforms will be required.

In conclusion, the BIN1 and DNM2 functional relationship is crucial for skeletal muscle integrity, and modulating BIN1 levels represents a therapy for dominant centronuclear myopathy.

Materials and Methods

Primary antibodies used were anti-DHPR (sc-514685), anti-BIN1 (2406 and 3623, rabbit; Institut de Génétique et de Biologie Moléculaire et Cellulaire [IGBMC]), and anti-DNM2 (2841, rabbit; IGBMC), which were generated on site at the polyclonal antibody facility of the IGBMC. Secondary antibodies against rabbit immunoglobulin G conjugated with horseradish peroxidase were purchased from Jackson ImmunoResearch Laboratories (catalog No. 111-036-045). The chemiluminescence kit was purchased from Pierce.

Constructs. pEGFP *BIN1*, pEGFP *BIN1* ΔSH3, pAAV-CMV (cytomegalovirus promoter)-*BIN1* derived from pAAV multiple cloning site (MCS) (Stratagene), pMyc *DNM2* WT, pMyc *DNM2* R465W, and plasmid: pGEX6P1, pVL1392. pEGFP *BIN1* is a EGFP-tagged human full-length isoform 8 cDNA. The construct pMyc *DNM2* WT and pMyc *DNM2* R465W is a myc-tagged human full-length cDNA.

Recombinant Proteins. Human BIN1 full-length and SH3 of BIN1 with GST tag (GST-BIN1 and GST-SH3) were produced from pGEX6P1 plasmid in *Escherichia coli* BL21. *E. coli* producing these recombinant proteins were induced with isopropyl β-D-1-thiogalactopyranoside (IPTG) (1 mM) for 3 h at 37 °C, centrifuged at 7,500 × *g*, and proteins were purified using Glutathione Sepharose 4B beads (GSH-resin). Human DNM2 protein was produced from pVL1392 plasmids in Sf9 cells with the baculovirus system as described previously (39). Briefly, a transfection was performed with the DNM2 plasmid to produce viruses. Sf9 cells were infected with viruses and grown for 3 d at 27 °C and then centrifuged at 2,000 × *g* for 10 min. DNM2 recombinant protein was purified with GST-SH3 of BIN1 bound to Glutathione-Sepharose 4B beads (GE Healthcare) as previously described (40). The proteins after the elutions were analyzed by 12% sodium dodecyl sulphate–polyacrylamide gel electrophoresis (SDS-PAGE).

For the in vitro binding assays of DNM2 with BIN1, extracts from bacteria overexpressing GST-BIN1 full-length or GST-SH3 were loaded on Glutathione Sepharose 4B beads, washed, and then beads were incubated for 1 h at 4 °C with or without purified human DNM2. After washing the resin was analyzed by 12% SDS-PAGE.

For the binding using muscle lysate, purified GST-SH3 of BIN1 was incubated with lysates of TA muscles from *Dnm2* $^{RW/+}$ mice. After three washings the eluates were loaded on SDS-PAGE gels, transferred to the nitrocellulose membrane, and Western blot with anti-DNM2 antibodies was done.

Liposomes Experiments. Liposomes were prepared mixing 5% PI(4,5)P2 (P-4516, Echelon Biosciences), 45% Brain Polar Lipids (141101C, Merck), and 50% phosphatidylserine (840035P, Merck) in a glass vial previously washed with chloroform. Then the chloroform was evaporated using nitrogen gas flow and placed for 2 h in a vacuum desiccator to create a transparent lipid film. The dried lipids were rehydrated using the GTPase buffer (20 mM Hepes, 100 mM NaCl, 1 mM $MgCl_2$, pH 7.4) to a final concentration of 1 mg/mL and went through three cycles of freezing (−80 °C) and defreezing (37 °C) each for 15 min maintaining the vial in the dark. The resulted liposomes were passed through 0.4-μm polycarbonate filters 11 times using an Avanti Mini Extruder. The liposomes were stored in the dark at 4 °C for a maximum of 24 h. Liposomes were diluted to 0.17 mg/mL in GTPase buffer and incubated with BIN1 and DNM2 as previously described (32). BIN1, DNM2, or BIN1 + DNM2 was diluted to 2.3 μM in the GTPase buffer. Ten microliters of liposome solution was prepared on Parafilm and absorbed on electron microscopy (EM) carbon-coated grids for 5 min at room temperature in a dark humid chamber. The EM grids were transferred on droplets of BIN1, DNM2, or BIN1 + DNM2 and incubated for 30 min at room temperature in the dark. The grids were incubated with 1 mM GTP for 5 min. Filter paper was used to remove the solution. The EM grids were negatively stained with 2% uranyl acetate.

In Cellulo Tubulation Assays. COS-1 cells were plated (ibidi plates) and grown in Dulbecco's Modified Eagle Medium (DMEM) + 1 g/L glucose + 5% fetal calf serum (FCS) to 70% confluence. Cells were transiently cotransfected with different concentrations of BIN1-GFP plasmid and DNM2-Myc or DNM2 RW-Myc using Lipofectamine 3000 mix (L3000-015 Thermo Fisher) reagents in accordance with the manufacturer's protocol. After 24 h of transfection, COS-1 cells were washed with phosphate-buffered saline (PBS) and fixed in 4% paraformaldehyde (PFA) diluted in PBS for 20 min. The cells were permeabilized with 0.2% Triton X-100 diluted in PBS and after washing, unspecific binding sites were blocked with 5% bovin serum albumin (BSA) in PBS for 1 h. Fixed cells were incubated with primary antibody anti-DNM2 diluted in 1% BSA overnight. The secondary antibodies anti-rabbit Alexa 594 were diluted 1:500 and incubated for 2 h. Cells were observed on a confocal microscope and only the cotransfected cells were considered. Cells with BIN1 tubules shorter than the tubule diameter were considered as having fragmented tubules.

Animals. The heterozygous *Dnm2*$^{RW/+}$ mouse line (C57BL/6J) was generated with an insertion of a point mutation in exon 11 (24). Tg*BIN1* mice (C57BL/6J) were obtained through integration of a human BAC encompassing the full BIN1 gene as previously described (23). To obtain *Dnm2*$^{RW/+}$ Tg*BIN1* mice, female *Dnm2*$^{RW/+}$ were crossed with Tg*BIN1* males. The homozygous *Dnm2*$^{RW/RW}$ Tg*BIN1* mice were generated crossing *Dnm2*$^{RW/+}$ females with *Dnm2*$^{RW/+}$ Tg*BIN1* males. We analyzed only male mice. Animals were maintained at room temperature under a 12-h dark cycle. Protocols were approved by an institutional review committee (#01594.02 and #201512041851445).

Mice Phenotyping. The phenotyping tests were conducted blinded and they were always performed by the same examiners in order to avoid stress and ensure reproducibility. The phenotyping experiments were conducted at the same part of the day for all the cohorts, and weekly experiments were performed on the same day of the week. The hanging test was performed every week from 3 wk to 8 wk for the mouse line *Dnm2*$^{RW/RW}$ Tg*BIN1* and every month from 1 to 7 mo for *Dnm2*$^{RW/+}$ Tg*BIN1* mice. Mice were suspended upside down from a grid for a maximum of 60 s and the test was repeated three times for each mouse at each timepoint. The graphs (Figs. 1B and 3B) present the average time of hanging on the grid. The rotarod test was conducted at 4 and 8 mo of age. The test was 5 d long. Day 1 was the training day when mice learned to run in accelerating mode on the rotarod. From days 2 to 5 mice were placed on the rotarod three times each day and they ran for a maximum of 5 min in an accelerating mode (4 to 40 rpm).

AAV Transduction of TA Muscle. The AAV serotype 9 expressing the human *BIN1* under the control of the cytomegalovirus promoter (AAV9-*BIN1*) was generated as previously described (20), as well as the AAV control (AAV9-Ctrl) without the *BIN1* cDNA. Intramuscular injections were performed in 3-wk-old male mice. Mice were anesthetized with ketamine (20 mg/kg) and 0.4% xylazine (5 μL/g of body weight) by intraperitoneal injection. The TA muscle was injected with 20 μL of 7×10^{11} viral genome/mL of AAV9-*BIN1* or AAV9-Ctrl diluted in PBS.

Histology. Transversal TA muscle cryosections of 8 μm were fixed and stained with H&E, NADH-TR, and SDH for histological analysis. Images were acquired using the Hamamatsu Nano Zoomer 2HT Slide Scanner. Fiber sizes were measured using Fiji software and fibers with abnormal SDH staining and nuclei position were counted using Cell Counter Plugin in Fiji software.

Tissue Immunolabeling. Transversal 8-μm cryosections were prepared from TA frozen in isopentane and stored at −80 °C. After defreezing, and three PBS washes, the sections were permeabilized with 0.5% PBS–Triton X-100 and saturated with 5% BSA in PBS. The primary antibody and the secondary antibody (anti-rabbit Alexa Fluor 488) were diluted 1:250 in 1% BSA.

Tissue Electron Microscopy. After dissection, TA was stored in 2.5% PFA and 2.5% glutaraldehyde in 0.1 M cacodylate buffer. The sections were observed by electron microscopy (20). The T-tubule circularity and the number of T-tubules with abnormal direction were measured manually using the Fiji program.

In Situ Muscle Force. The force production of the TA was assessed with the Competel300A Mouse Test System (Aurora Scientific). Mice were anesthetized through a triple shot mixture by intraperitoneal (IP) injection of domitor/fentanyl mix (2/0.28 mg/kg), diazepam (8 mg/kg), and domitor (0.28 mg/kg). The distal tendon was attached to the transducer while knees and feet were fixed. The sciatic nerve was stimulated by electric pulses with increasing frequency from 1 to 125 Hz to measure the maximal force, and the specific force (sPo) was calculated by dividing the maximal force by the muscle weight (in grams).

Protein Extraction and Western Blot. TA muscle was lysed in radioimmunoprecipitation assay (RIPA) buffer with 1 mM dimethyl sulfoxide, 1 mM phenylmethylsulfonyl fluoride, and mini ethylenediaminetetraacetic acid (EDTA)-free protease inhibitor mixture tablets (Roche Diagnostics) on ice. After having measured the protein concentration, the lysate was diluted and loading buffer (50 mM Tris·HCl, 2% SDS and 10% glycerol) was added. Samples were separated using 10% SDS-PAGE. After transfer to nitrocellulose membrane, the membrane was saturated using 5% milk for 1 h and incubated with primary antibody anti-BIN1 (1:1,000, 2406, rabbit IGBMC) overnight. Membranes were then incubated with secondary antibody against rabbit immunoglobulin G conjugated with horseradish peroxidase for 1 h at room temperature (1:10000, Jackson ImmunoResearch Laboratories, 111-036-045). Membranes were incubated with a chemiluminescence kit (Pierce) and the signal was visualized in an Amersham Imager 600 detector (GE Healthcare Life Science).

Statistical Analysis. All the data are expressed as mean ± SEM. GraphPad Prism software was used to make all the graphs. Statistical tests were performed using GraphPad Prism software. Student's *t* test was used to compare two groups when they followed a normal distribution. To compare more than two groups which followed a normal distribution, one-way ANOVA and Tukey's post hoc test were used. If the groups did not follow a normal distribution, no-parametric Kruskal–Wallis test and Dunn's post hoc test were applied. *P* value smaller than 0.05 was considered significant. The number of mice used for each experiment is indicated in the figure legends.

Data Availability. All study data are included in the article and/or supporting information.

ACKNOWLEDGMENTS. We thank Laura Picas and Nicolas Vitale for liposome preparation, Yann Herault for providing transgenic *BIN1* mice, Dr. Wilson and Dr. Johnston (PENN Vector Core) for providing AAV serotype 9 (plasmid PL-T-PV0008), and IGBMC platforms for animal house, imaging, molecular biology, and histology. This study was supported by INSERM, CNRS, Strasbourg University, Agence National de la Recherche (ANR) Dynather (ANR-18-CE17-0006-02), and ANR-10-LABX-0030-INRT, a French State fund managed by the Agence Nationale de la Recherche under the frame program Investissements d'Avenir ANR-10-IDEX-0002-02, the French infrastructure for integrated structural biology, ANR-10-INBS-05, Instruct-European Research Infrastructure Consortium, Association Française contre les Myopathies-Telethon, and Myotubular Trust and Sparks, The Children's Medical Research Charity.

1. B. Antonny *et al.*, Membrane fission by dynamin: What we know and what we need to know. *EMBO J.* **35**, 2270–2284 (2016).
2. M. Bitoun *et al.*, Mutations in dynamin 2 cause dominant centronuclear myopathy. *Nat. Genet.* **37**, 1207–1209 (2005).
3. S. M. Ferguson, P. De Camilli, Dynamin, a membrane-remodelling GTPase. *Nat. Rev. Mol. Cell Biol.* **13**, 75–88 (2012).
4. C. Kojima *et al.*, Regulation of Bin1 SH3 domain binding by phosphoinositides. *EMBO J.* **23**, 4413–4422 (2004).
5. E. Lee *et al.*, Amphiphysin 2 (Bin1) and T-tubule biogenesis in muscle. *Science* **297**, 1193–1196 (2002).
6. O. Daumke, A. Roux, V. Haucke, BAR domain scaffolds in dynamin-mediated membrane fission. *Cell* **156**, 882–892 (2014).
7. A. Hohendahl *et al.*, Structural inhibition of dynamin-mediated membrane fission by endophilin. *eLife* **6**, e26856 (2017).
8. H. Jungbluth, C. Wallgren-Pettersson, J. Laporte, Centronuclear (myotubular) myopathy. *Orphanet J. Rare Dis.* **3**, 26 (2008).
9. N. B. Romero, Centronuclear myopathies: A widening concept. *Neuromuscul. Disord.* **20**, 223–228 (2010).
10. A.-S. Nicot *et al.*, Mutations in amphiphysin 2 (BIN1) disrupt interaction with dynamin 2 and cause autosomal recessive centronuclear myopathy. *Nat. Genet.* **39**, 1134–1139 (2007).
11. J. Laporte *et al.*, A gene mutated in X-linked myotubular myopathy defines a new putative tyrosine phosphatase family conserved in yeast. *Nat. Genet.* **13**, 175–182 (1996).
12. D. Cassandrini *et al.*, Italian Network on Congenital Myopathies, Congenital myopathies: Clinical phenotypes and new diagnostic tools. *Ital. J. Pediatr.* **43**, 101 (2017).
13. J. M. Wilmshurst *et al.*, RYR1 mutations are a common cause of congenital myopathies with central nuclei. *Ann. Neurol.* **68**, 717–726 (2010).
14. J. A. Bevilacqua *et al.*, Recessive RYR1 mutations cause unusual congenital myopathy with prominent nuclear internalization and large areas of myofibrillar disorganization. *Neuropathol. Appl. Neurobiol.* **37**, 271–284 (2011).
15. I. Vandersmissen *et al.*, An integrated modelling methodology for estimating the prevalence of centronuclear myopathy. *Neuromuscul. Disord.* **28**, 766–777 (2018).
16. J. Böhm *et al.*, Mutation spectrum in the large GTPase dynamin 2, and genotype-phenotype correlation in autosomal dominant centronuclear myopathy. *Hum. Mutat.* **33**, 949–959 (2012).
17. O. S. Koutsopoulos *et al.*, Dynamin 2 homozygous mutation in humans with a lethal congenital syndrome. *Eur. J. Hum. Genet.* **21**, 637–642 (2013).
18. J. A. Kenniston, M. A. Lemmon, Dynamin GTPase regulation is altered by PH domain mutations found in centronuclear myopathy patients. *EMBO J.* **29**, 3054–3067 (2010).
19. L. Wang *et al.*, Dynamin 2 mutants linked to centronuclear myopathies form abnormally stable polymers. *J. Biol. Chem.* **285**, 22753–22757 (2010).
20. B. S. Cowling *et al.*, Increased expression of wild-type or a centronuclear myopathy mutant of dynamin 2 in skeletal muscle of adult mice leads to structural defects and muscle weakness. *Am. J. Pathol.* **178**, 2224–2235 (2011).
21. N. Liu *et al.*, Mice lacking microRNA 133a develop dynamin 2–dependent centronuclear myopathy. *J. Clin. Invest.* **121**, 3258–3268 (2011).
22. B. S. Cowling *et al.*, Amphiphysin (BIN1) negatively regulates dynamin 2 for normal muscle maturation. *J. Clin. Invest.* **127**, 4477–4487 (2017).
23. V. M. Lionello *et al.*, Amphiphysin 2 modulation rescues myotubular myopathy and prevents focal adhesion defects in mice. *Sci. Transl. Med.* **11**, eaav1866 (2019).
24. A.-C. Durieux *et al.*, A centronuclear myopathy-dynamin 2 mutation impairs skeletal muscle structure and function in mice. *Hum. Mol. Genet.* **19**, 4820–4836 (2010).
25. A. Fongy *et al.*, Nuclear defects in skeletal muscle from a Dynamin 2-linked centronuclear myopathy mouse model. *Sci. Rep.* **9**, 1580 (2019).
26. A. Toussaint *et al.*, Defects in amphiphysin 2 (BIN1) and triads in several forms of centronuclear myopathies. *Acta Neuropathol.* **121**, 253–266 (2011).
27. S. M. Sweitzer, J. E. Hinshaw, Dynamin undergoes a GTP-dependent conformational change causing vesiculation. *Cell* **93**, 1021–1029 (1998).
28. C. Spiegelhalter *et al.*, From dynamic live cell imaging to 3D ultrastructure: Novel integrated methods for high pressure freezing and correlative light-electron microscopy. *PLoS One* **5**, e9014 (2010).

29. M. Rosendale *et al.*, Functional recruitment of dynamin requires multimeric interactions for efficient endocytosis. *Nat. Commun.* **10**, 4462 (2019).
30. L. Picas *et al.*, BIN1/M-Amphiphysin2 induces clustering of phosphoinositides to recruit its downstream partner dynamin. *Nat. Commun.* **5**, 5647 (2014).
31. Y.-H. Chin *et al.*, Dynamin-2 mutations associated with centronuclear myopathy are hypermorphic and lead to T-tubule fragmentation. *Hum. Mol. Genet.* **24**, 5542–5554 (2015).
32. T. Takeda *et al.*, Dynamic clustering of dynamin-amphiphysin helices regulates membrane constriction and fission coupled with GTP hydrolysis. *eLife* **7**, e30246 (2018).
33. S. Neumann, S. L. Schmid, Dual role of BAR domain-containing proteins in regulating vesicle release catalyzed by the GTPase, dynamin-2. *J. Biol. Chem.* **288**, 25119–25128 (2013).
34. X. M. Muñoz, S. Buono, P. Koebel, J. Laporte, B. S. Cowling, Different in vivo impact of Dynamin 2 mutations implicated in Charcot-Marie-Tooth neuropathy or Centronuclear Myopathy. *Hum. Mol. Genet.* **28**, 4067–4077 (2019).
35. M. Zhao, L. Smith, J. Volpatti, L. Fabian, J. J. Dowling, Insights into wild-type dynamin 2 and the consequences of DNM2 mutations from transgenic zebrafish. *Hum. Mol. Genet.* **28**, 4186–4196 (2019).
36. S. Züchner *et al.*, Mutations in the mitochondrial GTPase mitofusin 2 cause Charcot-Marie-Tooth neuropathy type 2A. *Nat. Genet.* **36**, 449–451 (2004). Correction in: *Nat. Genet.* **36**, 660 (2004).
37. N. Sambuughin *et al.*, Adult-onset autosomal dominant spastic paraplegia linked to a GTPase-effector domain mutation of dynamin 2. *BMC Neurol.* **15**, 223 (2015).
38. Z. Ge *et al.*, Novel dynamin 2 mutations in adult T-cell acute lymphoblastic leukemia. *Oncol. Lett.* **12**, 2746–2751 (2016).
39. A. Quan, P. J. Robinson, Rapid purification of native dynamin I and colorimetric GTPase assay. *Methods Enzymol.* **404**, 556–569 (2005).
40. R. Kalia, N. Talledge, A. Frost, Structural and functional studies of membrane remodeling machines. *Methods Cell Biol.* **128**, 165–200 (2015).